Experimental and Numerical Investigations on Transition in a Laminar Separation Bubble

M. Lang, O. Marxen, U. Rist, S. Wagner
Universität Stuttgart, Institut für Aerodynamik und Gasdynamik (IAG)
Pfaffenwaldring 21, 70550 Stuttgart, Germany

Summary

A laminar boundary layer separates in a region of adverse pressure gradient on a flat plate, undergoes transition, and finally the turbulent boundary layer reattaches. Laminar-turbulent transition within this laminar separation bubble (LSB) is investigated by means of measurements with a Laser-Doppler-Anemometer (LDA), flow visualization in water and direct numerical simulation (DNS). The role of unsteady disturbances with and without controlled spanwise variation in the occuring mechanism of transition are examined in detail.

1 Introduction

The laminar water tunnel at the IAG was especially designed to study transition in Blasius boundary layers and in separation bubbles [1]. Because of the large scales in water, this water tunnel is particularly suitable for flow visualization. Wiegand et al. [2] and Kruse & Wagner [3] confirmed the high quality of the tunnel flow. Recent investigations on laminar separation include an experimental study of a LSB excited by an impulsive point-source disturbance [4]. Transition in a LSB employing DNS was examined in [5] with controlled forcing and in [6] without forcing. Despite these efforts to study LSB's, no detailed comparison of numerical results with experimental data obtained in a LSB has been made up to now, in particular for unsteady phenomena. In the present work it will be shown that by mutual comparison of results from calculations and measurements, mechanisms leading to the breakdown into turbulence in existing experimental facilities can be identified in a way that is not possible when applying only one of these methods.

2 Experimental and Numerical Methods

2.1 Experimental Set-Up

A flat plate with an elliptical nose is mounted in the test section of the laminar water tunnel. Optical access is permitted from all sides of the test section. A screen at the end of the flat plate leads to a pressure difference between the upper and the lower side of the flat plate. A gap between plate and sidewalls allows fluid transport beneath the plate. This prevents the formation of an unstable corner boundary layer, therefore extending the range of laminar flow on the plate. At a free stream velocity of $125\ \frac{mm}{s}$ a shape factor of $H_{12} = 2.6 \pm 1\%$ was measured.

New Results in Numerical and Experimental Fluid Mechanics III,
Contributions to the 12th STAB/DGLR Symposium Stuttgart, Germany 2000
S. Wagner, U. Rist, H.-J. Heinemann, R. Hilbig (Eds.)
Notes on Numerical Fluid Mechanics 77, Springer-Verlag 2002
pp. 207-214

To generate a pressure induced laminar separation bubble, a displacement body is positioned in the test section above the plate (Fig. 1). After a short region of favourable pressure gradient the adverse pressure gradient is applied. The boundary layer developing on the displacement body is sucked off at two suction stripes in streamwise direction to prevent separation and transition on the displacement body itself.

A 2-D Tollmien-Schlichting wave is generated by an oscillating wire which is positioned before the displacement body in the region of favourable pressure gradient. The frequency of this disturbance is $f_0 = 1.1\ Hz$. This is also the frequency which is most amplified according to linear stability theory. In the undisturbed case the separation bubble oscillates with the same frequency but not with a constant amplitude as in the case with disturbance input. The oscillating wire generates one trigger signal each period which is taken as time reference for the LDA-measurements. Therefore, the phases, wavelengths and phase velocities can be determined.

To investigate the development of a 3-D disturbance input and to fix appearing vortex structures in spanwise direction, thin ($1\ mm$) metal plates (spacers) are placed regularly underneath the wire. Interaction of the spacers with the oscillating wire results in a 3-D wave combination with typical peak-valley structure, where the boundary layer thickens in the peak plane compared to the valley plane [3, 7]. In the present measurements with 3-D disturbance input the spanwise wavelength was set to $\lambda_z = 58\ mm$, so that regularly appearing vortex structures could be seen in the transition region. For that purpose, visualizations using a hydrogen bubble technique and fluorescent colors in combination with Laser light sheets were carried out (Fig. 2).

The applied 2-D LDA measures the velocity components $\hat{U}(t)$ in mean flow direction and the vertical component perpendicular to the flat plate $\hat{V}(t)$. All velocities are non-dimensionalized by a velocity $\hat{U}_\infty$, taken in the narrowest section ($\hat{x} = 0\ mm$) at a wall-normal distance $\hat{y} = 50\ mm$, where $\hat{}$ denotes dimensional variables.

In order to achieve near-wall measurements with the probe aligned almost perpendicular to the side walls, the lower beam can be shifted to the optical axis of the probe. However, this halves the beam intersection angle for the vertical velocity component $\hat{V}$ thus causing a higher noise level compared to the streamwise component $\hat{U}$. The lowest turbulence level measurable with the LDA is 0.8% for the $\hat{U}$ velocity [3]. In contrast to hot-film anemometry, a LDA is a non-intrusive measurement technique which provides the possibility to identify velocities with their value and direction. In the transition region of the shear layer with its strong bidirectional velocity fluctuations, this is an important benefit. Thus, the dividing streamline can be determined directly from the measured velocity profiles.

2.2 Numerical Method and Calculation Parameters

Spatial direct numerical simulation (DNS) of incompressible flow is used to compute the pressure induced LSB described in the previous section. In the numerical method, fourth-order accurate finite differences are used for downstream and wall-normal discretization, while a spectral ansatz is applied in spanwise direction. A fourth-order Runge-Kutta scheme is used for time integration. Upstream of the outflow boundary a buffer domain smoothly returns the flow to a steady laminar state. The streamwise pressure gradient is imposed by prescribing a potential velocity distribution for the streamwise velocity u_p at a constant distance y from the wall, while the displacement effect of the boundary layer is captured by a boundary layer interaction model. The numerical method applied in this study is described in detail in [8]. A small-amplitude 2-D Tollmien-Schlichting (TS) wave is forced upstream of the LSB. Additional 3-D disturbances are excited to trigger the break-up of the separated shear layer into regions of small-scale turbulence.

Parameters of the flow are chosen to match the experimental setup introduced before. The length of the computational box in streamwise direction is $\hat{x} \approx 800\ mm$, with the inflow placed

at the position of the narrowest section (Fig. 1). The height of the box is $\hat{y} = 50\ mm$ in wall-normal direction, corresponding to approximately 12.5 times the displacement thickness δ_1 of the incoming boundary layer. In spanwise direction a single spacer wavelength fits into the domain ($\hat{z} = \hat{\lambda}_z = 58\ mm$). The resolution is 185 and 1778 grid points in wall-normal and streamwise direction, respectively. One TS wave is discretized with approximately 120 grid points. In spanwise direction 27 Fourier modes are computed. The resolution was confirmed to be sufficient by a calculation with increased number of grid points (approximately by a factor of 1.5 in each direction) yielding the same results in the first part of the LSB, which is discussed in this paper.

The velocity profile at the inflow boundary was obtained from a preceeding 2-D DNS of a strongly accelerated boundary layer (starting from a Blasius solution well upstream of the displacement body in the experiment) with the favorable pressure gradient chosen to match the experimental values up to the narrowest section, since the measured profile could not be represented by an analytical (Falkner-Skan) solution ($H_{12} \approx 1.6$ at the inflow). As can be seen in Fig. 3, the u-velocity profile from measurements and computations at $\hat{x} = 0\ mm$ are in excellent agreement. Hence, this profile is expected to be an appropriate inflow condition for the subsequent DNS of the LSB.

The potential velocity distribution u_p is chosen according to measurements where separation was suppressed by artificially causing transition prior to the laminar separation point (Fig. 3). It serves as initial condition at the free-stream boundary in the DNS and finally the mean edge velocity distribution u_e almost matches the experimental measurements with separation bubble. Since this velocity condition at the upper boundary is not fixed, but rather comes out of the boundary-layer interaction model, it can already be considered a result of the DNS. Good agreement of DNS data with experiments (Fig. 3) therefore gives a first prove of the comparability of the separation bubbles observed in the experiment and in the DNS. Furthermore, it should be emphasized that the actual velocity prescribed at the upper boundary is unsteady and the results presented in the diagram are time-averaged.

2.3 Data Analysis

In order to obtain the spanwise wavenumbers of the 3-D disturbance input, velocity profiles were measured in streamwise and spanwise direction. The resolution in span was 16 points per λ_z and the record length of all measured points was about 30 wire cycles. The time-signals are cut to multiples of the wire cycle time to evaluate the entire spectrum of the measured data.

For an exact determination of the amplitudes and phases of the oscillations in the flow a phase averaging technique with respect to the oscillating wire is used [3, 9]. A Fourier transformation in time followed by a transformation in spanwise direction yields the amplitudes $a_{h,k}$ and phases $\Phi_{h,k}$ of the disturbance [7].

$$\begin{aligned} u'(x,y,z,t) &= \sum_{h=1}^{H} a_h(x,y,z)\sin(h2\pi f_0 t + \phi_h(x,y,z)) \\ &= \sum_{h=1}^{H}\sum_{k=-K}^{K} a_{h,k}(x,y)\sin(h2\pi f_0 t - k\frac{2\pi}{\lambda_z}z + \phi_{h,k}(x,y)), \end{aligned}$$

The indices h and k represent the wave-number coefficients in time and spanwise direction and specify the (h,k)-modes of this double Fourier transformation. This method can be used until strong non-periodicities occur in the reattachment region of the laminar separation bubble.

In DNS, data from four TS cycles are Fourier analyzed in time using a Hanning window function to suppress the influence of low frequency drifting of the bubble. This drift would otherwise contaminate the Fourier-analyzed signals. The low level of subharmonic disturbances resulting

from this way of data processing confirms the clear distinction of drifting and TS frequency, supporting the validity of this procedure.

3 Results

In the present results the Reynolds number based on the displacement thickness at the separation line is about $Re_{\delta_1} = 900$. The extent of the transitional separation bubble of about $250\ mm$ is given by the mean dividing streamline with the net mass flux set to zero.

$$\int_{z=0}^{z_T} \bar{u}(z) dz = 0$$

First of all, general properties of the LSB are discussed using base flow variables. Here, base flow means averaged quantities in time and spanwise direction. Note that the LSB is a highly unsteady phenomenon, and the base flow can never be observed instantaneously at any timestep.

In Fig. 4 grayscale contours of the streamwise velocity are shown. The darkest color shows the reversed flow region bounded by the line of vanishing streamwise velocity ($u = 0$). Good agreement between DNS results and measurements reveals that a separation bubble of approximately the same size is formed in both cases. At the point of laminar separation S the dividing streamline (dash-dotted) moves away from the wall until the flow undergoes transition (around location T). It ends at point R, where the flow reattaches in the mean as a turbulent boundary layer. The mean recirculation vortex is illustrated by a closed streamline in the rear part of the separation bubble. In Fig. 5 a comparison of some boundary layer quantities is shown. Boundary layer thickness δ as well as displacement thickness δ_1 considerably increase along the separation bubble, while the momentum thickness δ_2 starts to grow not until the onset of transition. As expected from the streamwise velocity, results from experiment and DNS again correspond very well. Since the LSB is of unsteady character as emphasized before, it appears inevitable to compare time-dependent results before claiming that the same physics are captured in the numerical and experimental investigations. This shall be done in the next paragraph for 2-D quantities first.

The first section of the LSB is dominated by a primary convective instability of the 2-D TS wave (see [10]). The same holds for the size of the bubble.Therefore, the development of the 2-D TS wave appears to be very important and is examined in detail. Fig. 6 shows the amplification curve for the streamwise velocity. It can be seen that the TS wave $(1,0)$ is strongly amplified in the region of adverse pressure gradient. Experimental and numerical results perfectly match from $x = 230\ mm$ onwards even shortly beyond saturation. Good agreement with linear stability theory (LST) confirms the primary convective nature of the disturbance. Calculation and experiment also predict the same amplitude, growth rate and saturation level for the non-linearly generated higher harmonic disturbance $(2,0)$. The deviation of the amplitude development between experimental and DNS results up to $x = 230\ mm$ is probably due to a different kind of disturbance visible in the experiment. This disturbance is less damped than the TS wave in the accelerated region, therefore starting with higher initial amplitude into the region of adverse pressure gradient, until the TS mode catches up and its amplitude outnumbers all other perturbations. This is supported by the fact that the disturbance observed in the experiment halves its wavelength at the position of the sharp bend in the amplification curve. Disturbances in DNS are generated at a streamwise position where the TS mode is already the most amplified disturbance and therefore correspond to linear stability theory from the beginning.

Wall-normal distributions of amplitudes and phases for the streamwise velocity u and wall-normal velocity v are shown in Fig. 7 at a location in the middle of the region of linear amplification. In the lower part of the base flow profile the reversed flow is clearly visible. The

detached shear layer corresponds to the part of maximum streamwise velocity gradient around $y = 13\ mm$. It is at this distance from the wall where the disturbance amplitude of the 2-D TS wave reaches maximum values for the u-velocity.

In the experiment, a strong steady disturbance with half the spacer wavelength (0,2) can be observed (Fig. 8). From good agreement with LST for the development of the 2-D TS wave as described in the previous section it can be concluded that the spanwise modulation of the base flow does not exert any influence on 2-D instability characteristics of the flow field. In contrast, the growth of spanwise modulated perturbations of fundamental frequency is decisively affected by the presence of this steady mode. Strong growth of these disturbances cannot be explained by linear theory, which would give considerably lower growth rates, nor by a secondary (convective [11] or temporal [10]) instability, since it already sets in well before the TS wave has gained a sufficient amplitude. DNS calculations in which a similar steady perturbation was excited (see Fig. 8 and amplitude distribution Fig. 9) revealed that the growth rate of mode (1,2) can be explained by non-linear generation, though the amplitude level in the DNS and the experiment are different. Interaction of disturbances (0,2) and (1,0) produces a mode (1,2) that exhibits the same growth rate as the one observed in the measurements (Fig. 8). Agreement of amplitude and phase distributions between experiment and DNS is reasonable (Fig. 9), albeit deviation from symmetry can be seen in the measurements, which are not included in the DNS method in this study. Despite the importance of 3-D disturbances for the breakdown to turbulence, the dominance of the 2-D fundamental perturbation even far downstream of reattachment is remarkable [10].

4 Conclusions

A detailed comparison between measurements and numerical calculations of the velocity field in a transitional separation bubble showed very good agreement for time-averaged and 2-D Fourier analyzed quantities. Transition in a separation bubble under consideration here is driven by convective primary amplification of 2-D TS waves, mainly determining the size and position of the bubble. This mechanism could be clearly identified from the existing numerical and experimental data. The same holds for the formation of spanwise variations of the incoming 2-D flow field, which can be attributed to large steady perturbations and non-linearly generated time-dependent disturbances. The influence of the amplitude of these disturbances, which differed between experiment and DNS remains open to further investigation.

Acknowledgements: The financial support of this research by the Deutsche Forschungsgemeinschaft DFG under grant Wa 424/19-1 is gratefully acknowledged.

References

[1] Strunz, M. and Speth, J. F., A new laminar water tunnel to study the transition process in a Blasius boundary layer and in a separation bubble and a new tool for industrial aerodynamics and hydrodynamic research. *AGARD CP-413*, pp. 25–1–25–5 (1987).

[2] Wiegand, T., *Experimentelle Untersuchungen zum laminar-turbulenten Transitionsprozess eines Wellenzuges in einer Plattengrenzschicht*. Dissertation, Universität Stuttgart (1996).

[3] Kruse, M. and Wagner, S., LDA Measurements of Laminar-Turbulent Transition in a Flat-Plate Boundary layer. 8th International Symposium on Applications of Laser Techniques to Fluid Mechanics, 8.–11. July, Lisbon, Portugal (1996).

[4] Watmuff, J., Evolution of a wave packetinto vortex loops in a laminar separation bubble. *J. Fluid Mech.*, 397, 119–169 (1999).

[5] Alam, M. and Sandham, N. D., Direct numerical simulation of 'short' laminar separation bubbles with turbulent reattachment. *J. Fluid Mech.*, 410, 1–28 (2000).

[6] Spalart, P. and Strelets, M. K., Mechanisms of transition and heat transfer in a separation bubbles with turbulent reattachment. *J. Fluid Mech.*, 403, 329–349 (2000).

[7] Kruse, M., *Einsatz der Laser-Doppler-Anemometrie zur Untersuchung des laminar-turbulenten Grenzschichtumschlags an der ebenen Platte*. Dissertation, Universität Stuttgart (1997).

[8] Maucher, U., Rist, U. and Wagner, S., Refined Interaction Method for Direct Numerical Simulation of Transition in Separation Bubbles. *AIAA Journal.*, **38(8)**, 1385–1393 (2000).

[9] Lang, M., Marxen, O., Rist, U., Wagner, S. and Würz, W., LDA-Messungen zur Transition in einer laminaren Ablöseblase. In: *Lasermethoden in der Strömungmeßtechnik*. 8. Fachtagung der GALA, 12.–14. Sep. 2000, Freising-Weihenstephan, FRG, Shaker Verlag, Aachen (2000).

[10] Maucher, U., Rist, U. and Wagner, S., Transitional Structures in a Laminar Separation Bubble. In: W. Nitsche, H. Heinemann and R. Hilbig (eds.), *Notes on Numerical Fluid Mechanics*, vol. 72, pp. 307–314. Vieweg Verlag, Wiesbaden (1999), 11^{th} Stab Symposium 98, Berlin.

[11] Rist, U., *Zur Instabilität und Transition in laminaren Ablöseblasen*. Habilitation, Universität Stuttgart, Shaker Verlag, Aachen (1998).

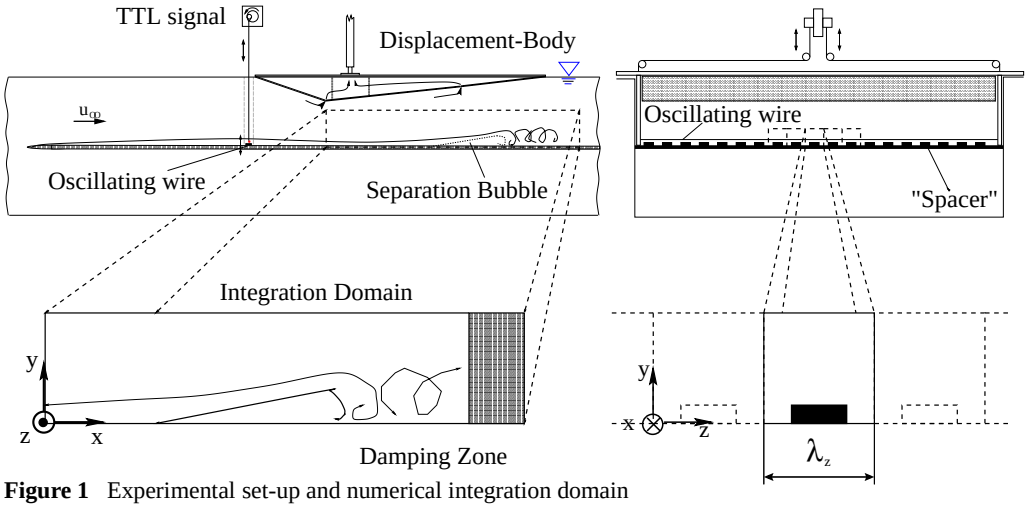

Figure 1 Experimental set-up and numerical integration domain

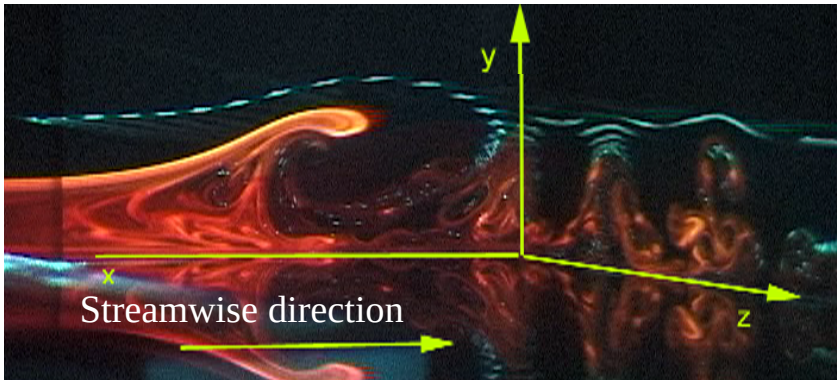

Figure 2 Flow visualization of the transition region. 2 simultaneous Laser light sheets in xy-plane (Peak-Position) and yz-plane (x=330 mm), respectively.

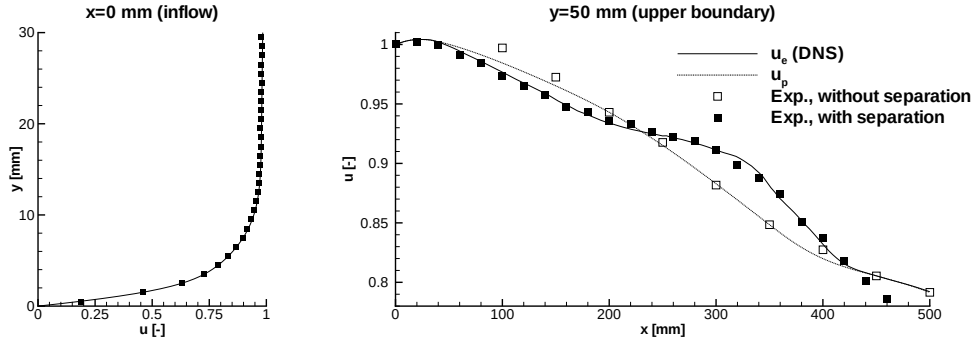

Figure 3 Streamwise mean velocity at $\hat{x} = 0\ mm$ (left) and $\hat{y} = 50\ mm$ (right). DNS results u_e (solid line), potential velocity u_p prescribed in DNS (dotted line); Measurements with (filled symbols) and without separation (open symbols).

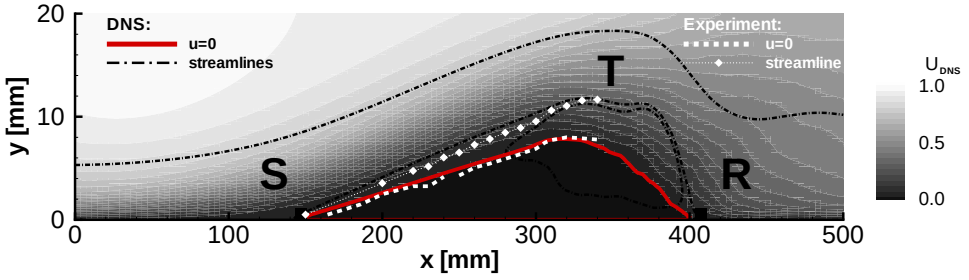

Figure 4 Contours of streamwise mean velocity (averaged in time and span) together with lines $u = 0\ mm$ and streamlines.

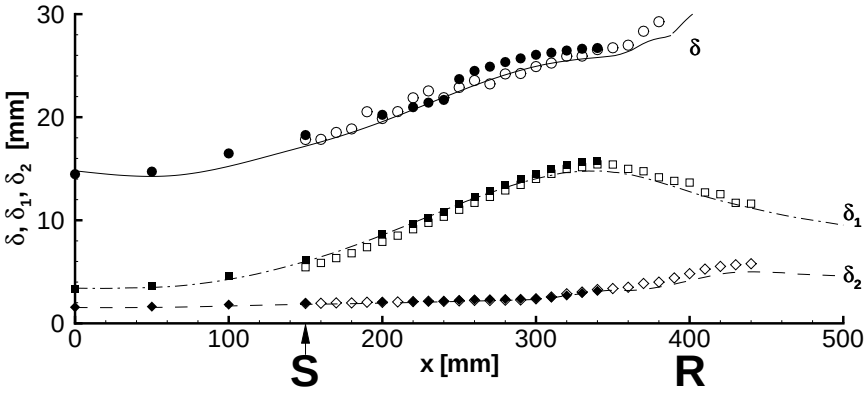

Figure 5 Time-averaged boundary layer quantities in the vicinity of a LSB. Results from spanwise-averaged DNS (lines) and measurements with spacer and spanwise-averaging (filled symbols) and without spacer at a single spanwise position (open symbols).

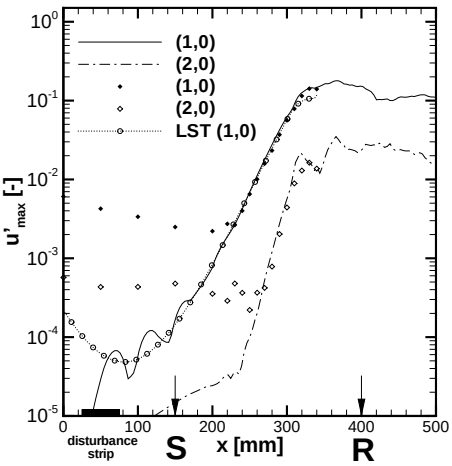

Figure 6 Amplification of the maximum velocity fluctuation u'_{max}. Results from DNS (lines), measurements (symbols) and LST.

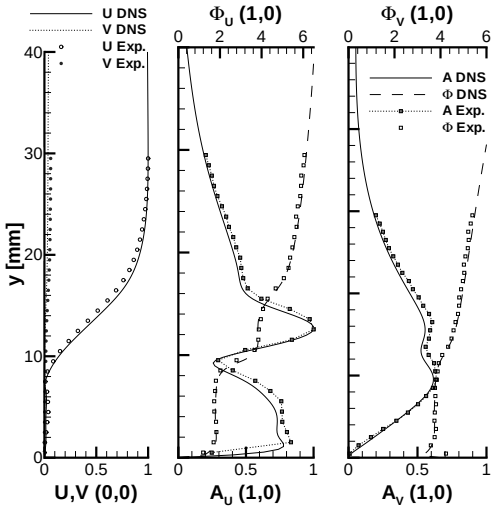

Figure 7 Normalized 2-D amplitude and phase distributions. Results from DNS (lines) and measurements (symbols) at $x = 290\ mm$.

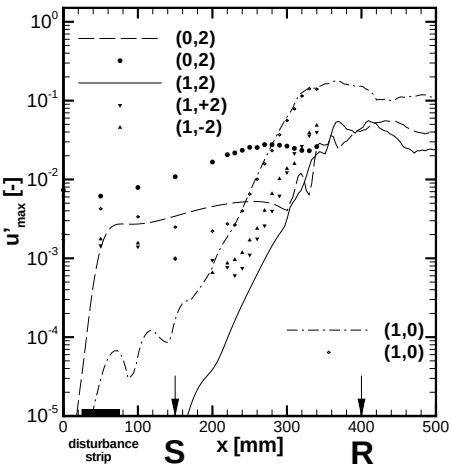

Figure 8 Amplification of the maximum velocity fluctuation u'_{max}. Results from DNS (lines) and measurements (symbols).

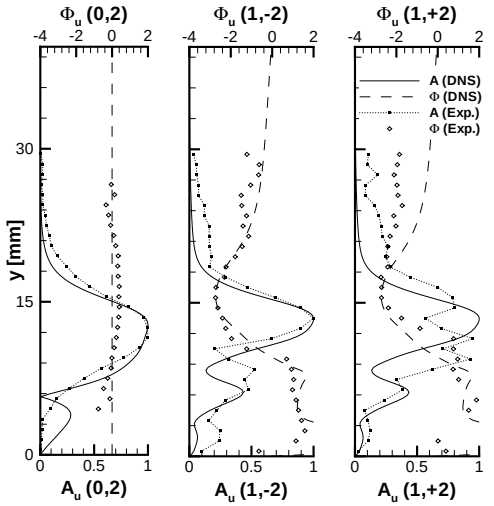

Figure 9 Normalized 3-D amplitude and phase distributions. Results from DNS (lines) and measurements (symbols) at $x = 290\ mm$.